Møller Scattering Polarimetry
for
High Energy e$^+$e$^-$ Linear Colliders

GIDEON ALEXANDER[1,2]

Institut für Physik

Humboldt-Universität zu Berlin, Germany

11015 Berlin, Germany

and

IULIANA COHEN[3]

School of Physics and Astronomy

Raymond and Beverly Sackler Faculty of Exact Sciences

Tel-Aviv University, Tel-Aviv 69978, Israel

Abstract

The general features of the Møller scattering and its use as an electron polarimeter are described and studied in view of the planned future high energy e^+e^- linear colliders. In particular the study concentrates on the TESLA collider which is envisaged to operate with longitudinal polarised beams at a centre of mass energy of the order of 0.5 TeV with a luminosity of about $\mathcal{L} = 10^{34}$ cm^{-2}sec^{-1}.

---

[1]On Sabbatical leave from Tel-Aviv University.

[2]e-mail: alex@lep1.tau.ac.il.

[3]e-mail: cohen@lep1.tau.ac.il

1 Introduction

It is for some time that the high energy physics community is of the opinion that in the near future there will be a need for the facility of a high energy linear e^+e^- collider with a nominal energy around 0.5 TeV in the centre of mass (CM) system. A conceptual design of such a collider, known under the name TESLA, and its physics program is described in some details in Ref. [1]. It has further been pointed out that the option of longitudinal polarized electron beams in such high energy colliders, like TESLA, will enrich significantly the physics capabilities of the device [2]. The use of polarised beams requires however a continuous monitoring and sufficient accurate measurement of the beam polarisation during the entire collider operation.

In addition to the widely used Compton scattering polarimeter, the $e^-e^- \to e^-e^-$ Møller scattering process has also been utilised to evaluate the polarisation level of the electron beams. Unlike the Compton polarimeter the operation of a Møller polarimeter may need dedicated accelerator runs but its relatively simple construction and operation and the large counting rates makes it nevertheless a rather attractive device. Here one should note that the method applied for the Møller polarimeter can also be applied almost without any change to the measurement of a positron beam polarisation by replacing the Møller process with the Bhabha scattering [3].

Several colliders have in fact already used Møller polarimeters to monitor their polarized electron beams. The Stanford Linear Collider (SLC) has primarily used a precise Compton polarimeter to monitor the beam and measure the electron beam polarisation [4, 5]. In addition it has also engaged two single-arm Møller polarimeter for beam polarisation diagnosis. Many fixed target experiments, e.g. those described in references [6–9], were running with polarised beams monitored by Møller polarimeters. Finally the Møller like scattering, $\mu e \to \mu e$, was used in the SMC experiment at CERN [10] to measure the polarisation of the muon beam. The Møller measurement can be also be carried out after the colliding beams interaction point (IP). From this point of view, the Møller polarimeters are more suited for the NLC, JLC or CLIC linear colliders, than for TESLA, because of the non-zero crossing, the extraction does not require bending of the electron trajectories after the IP.

In this paper we describe the outcome of a detailed study which explored the feasibility and possibility to use the Møller scattering process as a method for the longitudinal polarisation measurement of the TESLA electron beam. In Sections 2 and 3 we describe in some details the various properties of the Møller scattering, with and without polarised beams, and also review some of the technical characteristics of the Møller polarimeters used in recent high energy experiments emphasizing the specific TESLA needs. The expected event rates and the effects of the energy deposition in the target by the electron beam are dealt with in Section 4. In Section 5 we consider two somewhat different methods for the beam polarisation measurement and evaluate their envisaged performance.

2 The Møller scattering

2.1 The basic formulae

The lowest order $e^- e^- \rightarrow e^- e^-$ Møller elastic scattering diagrams are the t-channel and u-channel γ exchanges[4] shown in Fig. 1. Each of these two diagrams contributes to the two possible spin configurations of the initial electrons, namely the parallel and anti-parallel states. From the Fermi-Dirac statistics follows that the relative phase between the two diagrams is negative. This has important consequences on the spin dependence of the cross section. For the anti-parallel spin configuration the scattered spins are also anti-parallel. The anti-parallel spin state contains an additional negative phase between the two possible orientations of the outgoing spins. As a result the amplitudes add and the cross section is larger for anti-parallel spin configuration generating a non-zero asymmetry.

The Møller differential elastic cross section at tree level and in the CM system is given by:

$$\frac{d\sigma}{d\Omega}(s) = \frac{\alpha^2}{s} \frac{(3 + \cos^2 \theta)^2}{\sin^4 \theta} \left\{ 1 - P_L^B P_L^T A_L(\theta) - P_t^B P_t^T A_t(\theta) \cos(2\phi - \phi_B - \phi_T) \right\}, \tag{1}$$

for high $E_{CM}^2 = s$ values so that the electron mass squared m_e^2 can be neglected.

---

[4]Despite the high energy of the beam in the laboratory system, the $\sqrt{s}$ is less than 1 GeV therefore the Z^0 gauge boson exchange contribution is negligible.
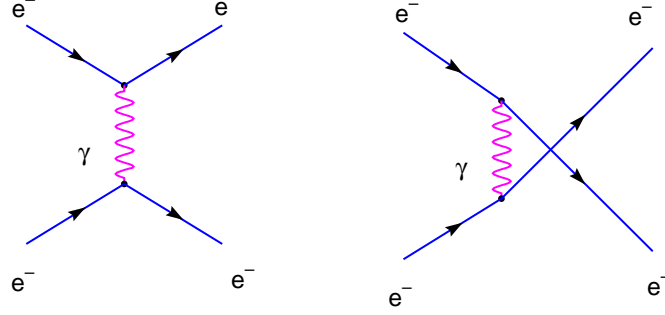
Figure 1: The lowest order Feynman diagrams describing the Møller elastic scattering.

Here:

α = the fine structure constant at low energies which is equal to 1/137;

θ = the CM frame polar scattering angle;

ϕ = the CM azimuthal angle of the scattered electron;

P_L^B and P_L^T = longitudinal polarisation of the beam and target;

P_t^B and P_t^T = transverse polarisation of the beam and target;

ϕ_B and ϕ_T = the azimuthal angles of the beam and target transverse polarisation vectors.

The longitudinal and transverse asymmetry functions, $A_L(\theta)$ and $A_t(\theta)$, are defined as:

$$A_L(\theta) = \frac{(7 + \cos^2 \theta) \sin^2 \theta}{(3 + \cos^2 \theta)^2} \quad \text{and} \quad A_t(\theta) = \frac{\sin^4 \theta}{(3 + \cos^2 \theta)^2} \quad (2)$$

and shown as a function of $\cos \theta$ in Fig. 2. To note is that both $A_L(\theta)$ and $A_t(\theta)$ are small in the forward direction so that the asymmetries are small in the region where the t-channel diagram dominates.

In order to determine the beam polarisation, the rate of the electrons scattered in a given solid angle $d\Omega$ is measured in one orientation of the beam and target polarisation vectors $(\vec{P}^B, \vec{P}^T)$ and then with the beam polarisation vector inverted i.e., $(-\vec{P}^B, \vec{P}^T)$. Here the polarisation vectors are defined as $\vec{P}^B \equiv [P_L^B, P_t^B]$ for the beam and $\vec{P}^T \equiv [P_L^T, P_t^T]$ for the target. The longitudinal component, P_L, is in the z-direction and P_t, the transverse component, is perpendicular to that direction. Thus the two rates which one measures are:
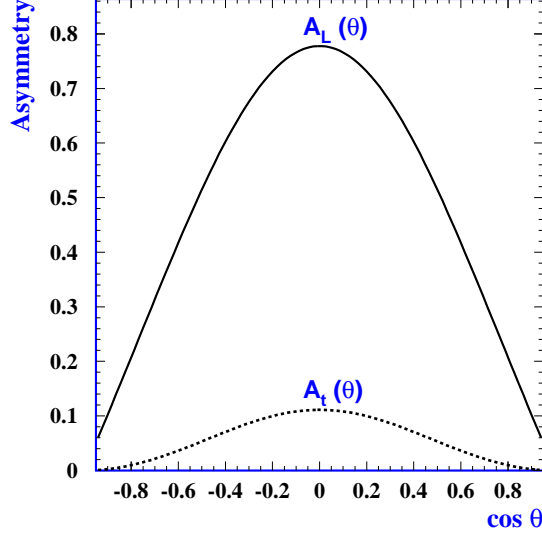
Figure 2: The longitudinal and the transverse asymmetry values A_L and A_t are plotted as a function of $\cos\theta$.

$$R(s, \vec{P}^B, \vec{P}^T) \qquad \text{and} \qquad R(s, -\vec{P}^B, \vec{P}^T),$$

normalised to the same integrated luminosity. From these rates one constructs the asymmetry A_R which is equal to:

$$A_R \equiv \frac{R(s, \vec{P}^B, \vec{P}^T) - R(s, -\vec{P}^B, \vec{P}^T)}{R(s, \vec{P}^B, \vec{P}^T) + R(s, -\vec{P}^B, \vec{P}^T)} = -P_L^B P_L^T A_L(\theta) - P_t^B P_t^T A_t(\theta) \cos(2\phi - \phi_B - \phi_T) \tag{3}$$

Finally the beam polarisation is extracted from the measured values of A_R, the measured target polarisation and the unpolarised asymmetry functions given in Eq. 2.

The expressions given in Eqs. 1 and 3 are derived for the lowest order diagrams for the $e^- e^- \to e^- e^-$ process. The contributions of higher diagrams, up to order 4 in the fine structure constant α, were in the past investigated in [11] and more recently in [12]. The QED corrections to the Møller asymmetry can be evaluated through the BMOLLR code developed by S. Jadach and B. Ward [13]. This is

4

an $\mathcal{O}(\alpha)$ exponentiated Monte Carlo generator for $e^-e^- \rightarrow e^-e^- + n\gamma$ with any n value.

2.2 Some general features

Some obvious features of the Møller scattering can be deduced from Eq. 1.

a) The cross section is seen to diverge at $\cos\theta = \pm 1$. This is due to the fact that the electron mass was neglected. In a rigorous treatment, where m_e is not neglected, the Møller scattering formula remains finite even at $\cos\theta = \pm 1$.
b) The cross section magnitude decreases as s increases, similar to the one photon annihilation process in e^+e^- annihilation.
c) Only if the beam and the target are simultaneously transverse and/or longitudinal polarised a change in the Møller scattering will be observed.
d) In the absence of transverse polarisation the cross section is independent of the azimuthal angle ϕ. This independence can also be achieved by integrating over the whole azimuthal angle ϕ provided of course that the experimental setup is ϕ independent.
e) The asymmetry functions reach their maximum at a CM scattering angle of 90° and approach zero in the forward and backward directions.

2.3 Differential cross sections and asymmetries

The cross sections and asymmetries were studied for a set of E_B values and several beam-target polarisation configurations where we set everywhere $\phi_B + \phi_T$ to zero. In order to illustrate the effects of the beam and target polarisations we assume for the target a polarisation of 90% realising that in practice an iron target has a maximum polarisation of 8%. The beam polarisation was taken to be 90%. In Fig. 3 we show, after integrating over the whole azimuthal angle ϕ, typical CM polar angular distributions of the Møller scattering at different beam energies scattered by a stationary electron target, without and with longitudinal polarisation characterised by their $P_L^B P_L^T$ values. For beam electrons of $E_B = 250$ GeV scattered over a stationary electron, we show in Fig. 4 the two dimensional plots of the Møller differential cross section $d^2\sigma/(d\cos\theta d\phi)$ with and without longitudinal polarisation and without and with transverse polarisation. In Fig.
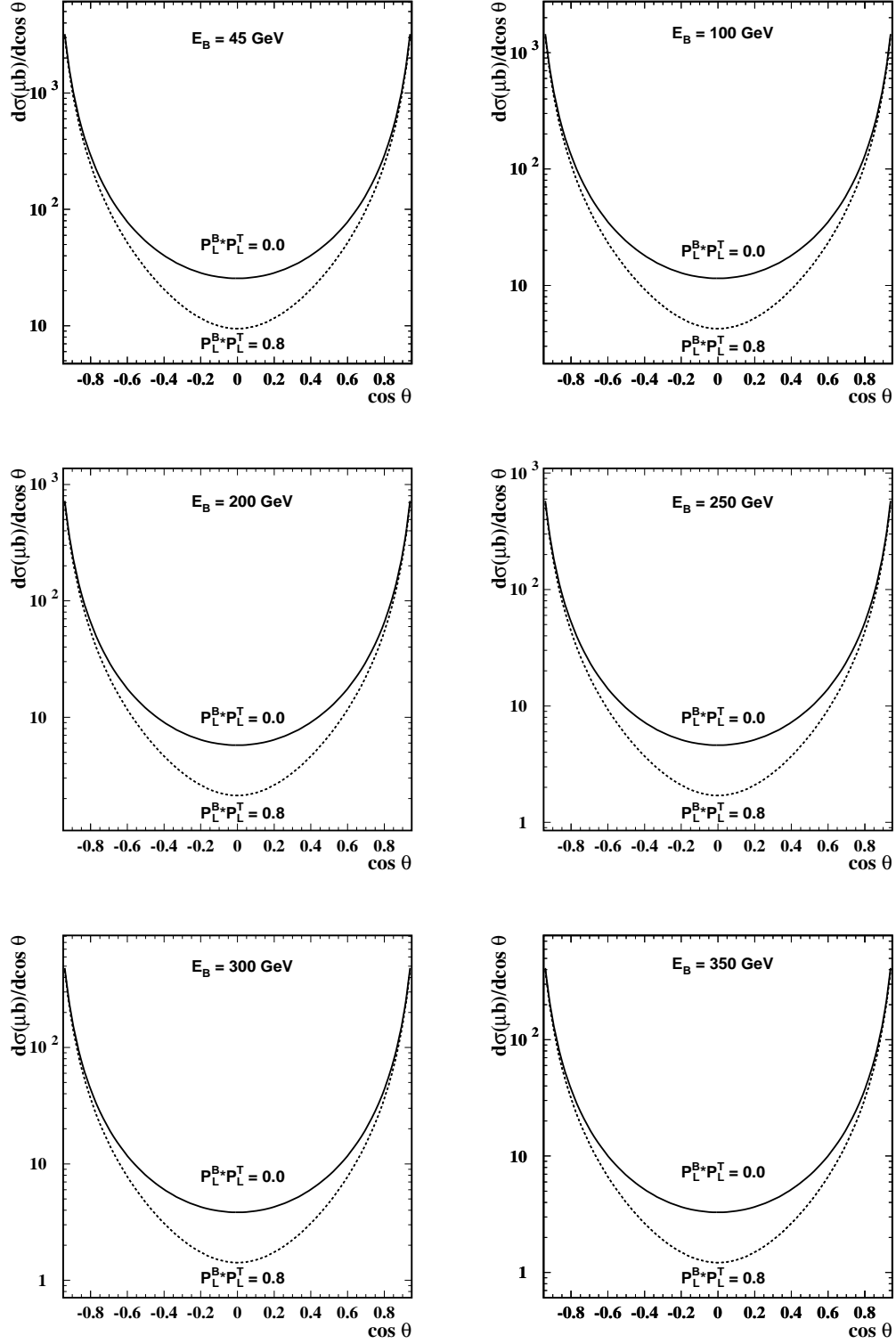
Figure 3: Møller differential cross section, $d\sigma/d\cos\theta$, as a function of $\cos\theta$ in the range of $|\cos\theta| < 0.9$ for several E_B and without and with longitudinal polarisation.
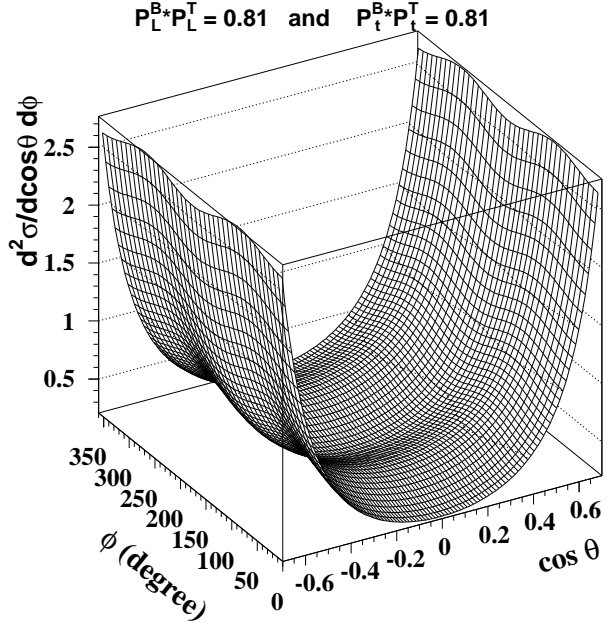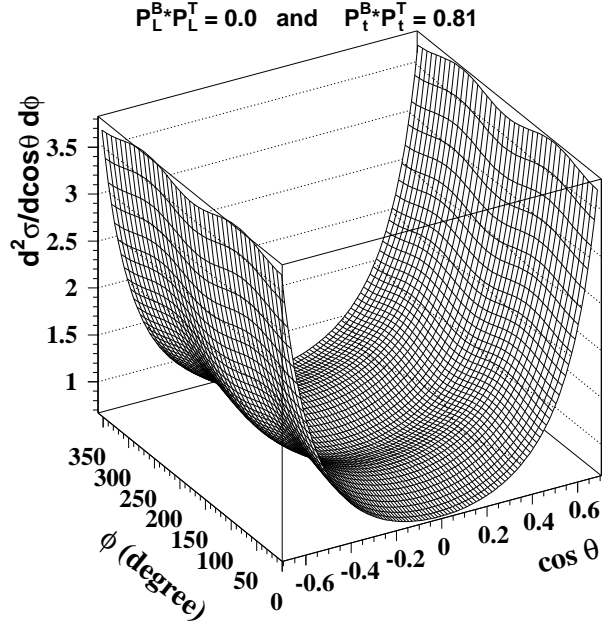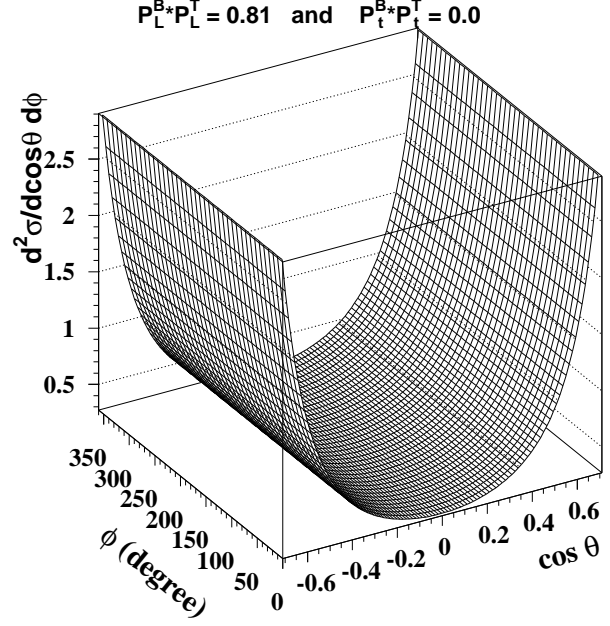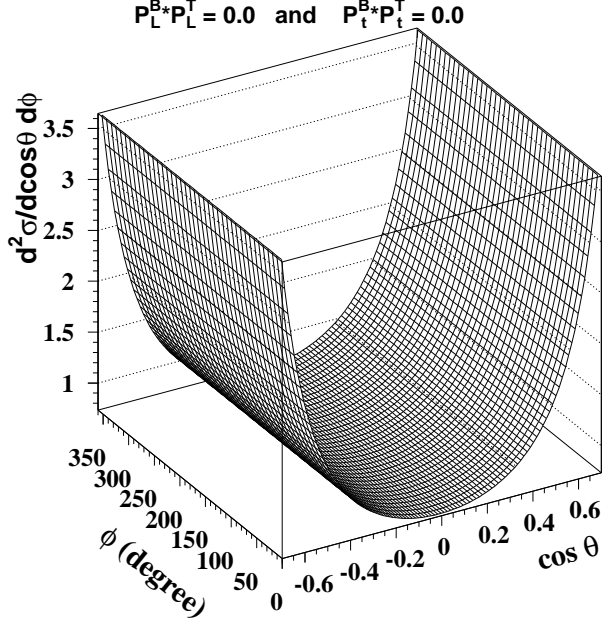
6

Figure 4: The 2-dimensional plots of $d^2\sigma(e^- e^- \rightarrow e^- e^-)/(d\cos\theta d\phi)$ in μb, at $E_B = 250$ GeV, are shown for several values of the longitudinal and transversal polarisations as indicated in the figures.
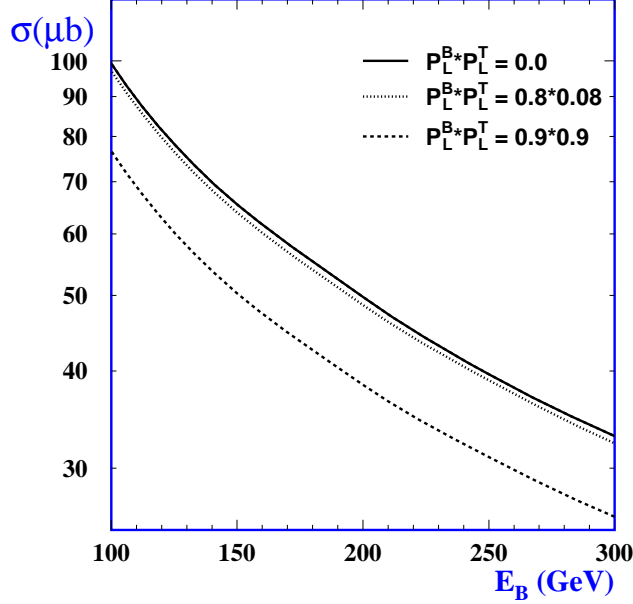
Figure 5: The total Møller scattering cross section, integrated over the range $0^o < \phi < 360^o$ and $|\cos\theta| < 0.9$, as a function of the beam energy without and with longitudinal polarisation. The target electron is taken to be at rest.

5 we show the total Møller cross section integrated over ϕ from 0° to 360° and over the polar angle region $|\cos\theta| < 0.9$ for unpolarised and polarised beam and target. Finally we show in Fig. 6(left) the Møller scattering asymmetry A_R as a function of $\cos\theta$ and ϕ for a longitudinal polarisation value of $P_L^B P_L^T = 0.81$ and $P_t^B P_t^T = 0.81$. In the same figure we also show the asymmetry A_R dependence on $\cos\theta$ after integrating over the ϕ angle.

3   Møller scattering in the laboratory system

In the collision of two electrons the total centre of mass energy squared s is written in the Lorentz invariant form, and thus valid in any reference system, as:

$$s = 2m_e^2 + 2E_B E_T(1 - \beta_B \beta_T \cos\theta_{1,2}) \, , \tag{4}$$

where E_B and E_T are the beam and target electron energies, $\theta_{1,2}$ is the angle between the incident particle's momenta and $\beta_{B,T} = p_{B,T}/E_{B,T}$ are the velocities
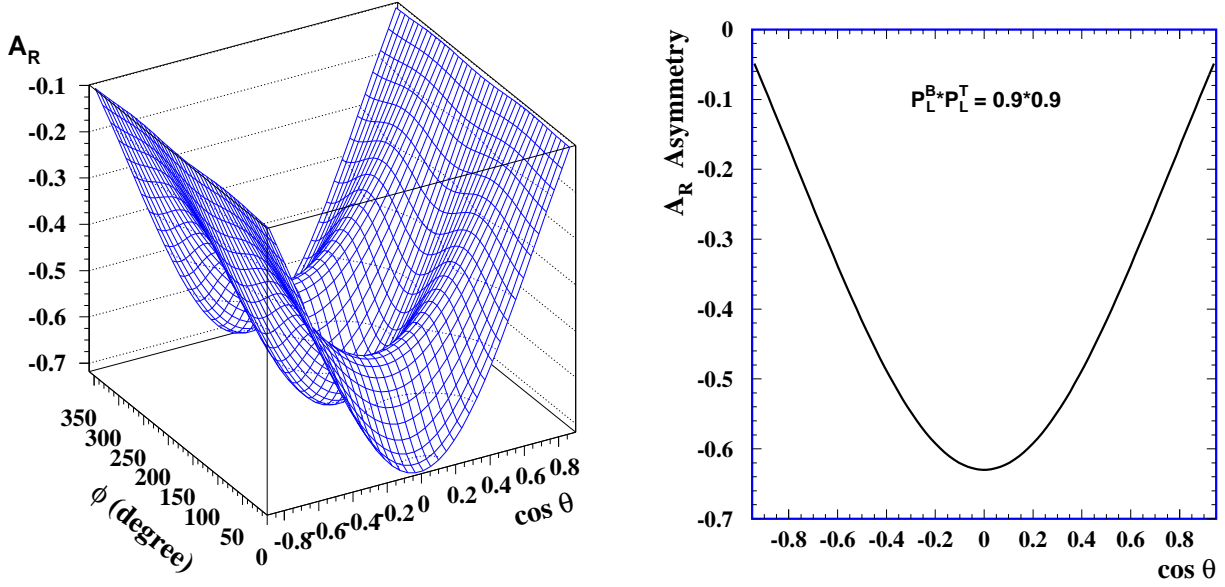
Figure 6: The Møller scattering asymmetry A_R in the CM system. Left, a 2-dimensional plot of A_R as a function of $\cos\theta$ and the azimuthal angle ϕ for $P_L^B P_L^T = 0.81$ and $P_t^B P_t^T = 0.81$. Right, A_R as a function of $\cos\theta$, integrated over $0^o < \phi < 360^o$, the beam and target polarisations values are indicated in the figure.

of beam and target electrons.

At TESLA, where the beam energy is planned to be a few hundreds GeV, one has $\beta_B = p_B/E_B \simeq 1$ so that one can neglect m_e^2 and Eq. 4 reduces to:

$$s = 2E_B E_T (1 - \beta_T \cos \theta_{1,2}) . \tag{5}$$

3.1 Target electrons at rest

In the approximation that the target electron is in the laboratory system a free particle at rest ($\beta_T = 0$), the square of the centre of mass energy, s_0, is given by the expression:

$$s_0 = 2E_B m_e = 2p_B m_e , \tag{6}$$

where p_B is the beam momentum and m_e is the electron mass. The laboratory momentum of the scattered electron , p_{lab}, is given by :

$$p_{lab} = \gamma_{\mathrm{CM}} \sqrt{(E^* + p^* \beta_{\mathrm{CM}} \cos \theta)^2 - \frac{m_e^2}{\gamma_{\mathrm{CM}}^2}} , \tag{7}$$

where p^*, E^* are the momentum and energy of the incident electron in the CM system and $\gamma_{\mathrm{CM}} = 1/\sqrt{1 - \beta_{\mathrm{CM}}^2}$. The relation between the laboratory scattering angle θ_{lab} and the CM scattering angle θ is given by:

$$\tan \theta_{lab} = \frac{1}{\gamma_{\mathrm{CM}}} \times \frac{\sin \theta}{\rho + cos\theta} , \tag{8}$$

where $\rho = \beta_{\mathrm{CM}}/\beta^*$ is the ratio of the velocity of the center of mass system and the velocity of the electron in the CM system. For elastic scattering of a beam electron of $E_B =$ 250 GeV on an electron at rest one has $m_e/E_B = 2 \times 10^{-6} << 1$ so that Eqs. 7 and 8 can be reduced to a simpler form.

Using the relation between β_{CM} and γ_{CM} and remembering that

$$\beta_{\mathrm{CM}} = p_B/(E_B + m_e)$$

one obtains:

$$\gamma_{\mathrm{CM}} = \sqrt{(E_B + m_e)/2m_e} . \tag{9}$$

In the CM system of the Møller scattering the momentum and energy of the incident electron are expressed by:

$$p^* = m_e \sqrt{\frac{E_B^2 - m_e^2}{2m_e^2 + 2E_B m_e}} = \sqrt{\frac{m_e(E_B - m_e)}{2}} \qquad (10)$$

$$E^* = m_e \frac{E_B + m_e}{\sqrt{2m_e^2 + 2E_B m_e}} = \sqrt{\frac{m_e(E_B + m_e)}{2}} \cdot \qquad (11)$$

Therefore

$$\beta^* = \frac{E_B - m_e}{E_B + m_e} \quad \text{and} \quad \rho = \frac{p_B}{E_B - m_e} \cdot \qquad (12)$$

Here β^* is the velocity of the incident electron calculated in the CM system. Using Eqs. 6, 9 and 12 we rewrite Eq. 7 to be:

$$p_{lab} = \frac{p_B}{\sqrt{s_0}} \times \frac{\sqrt{s_0}}{2}(1 + \cos\theta) = \frac{p_B}{2}(1 + \cos\theta) \cdot \qquad (13)$$

From this last equation follows that the momentum of the scattered electron does not depend on the CM total energy, but only on the beam energy and the CM scattering angle. From Eq. 8 one obtains, in a few simple steps, the expression:

$$\tan^2\theta_{lab} = \frac{2m_e}{E_B + m_e} \times \frac{1 - \cos\theta}{1 + \cos\theta} \cdot \qquad (14)$$

Finally in the small angle approximation, where $\tan^2\theta_{lab} \simeq \theta_{lab}^2$, one obtains from Eqs. 13 and 14 that

$$\theta_{lab}^2 = 2m_e \left(\frac{1}{p_{lab}} - \frac{1}{p_B}\right) \cdot \qquad (15)$$

The single-arm Møller polarimetry is based on Eq. 15 which provides the identification of the elastic $e^- e^-$ scattering through the relation, in the laboratory system, between θ_{lab} and p_{lab}. In Fig. 7 we show the relation between the centre of mass polar angle θ and the angle of scattered electron θ_{lab}, for three different E_B values.

The analysing power of the Møller polarimeter is proportional to the product of the unpolarized cross section and the square of the asymmetry [4]. The optimal scattering angle for polarimetry is thus the one that maximizes the analysing power of the method. For longitudinal polarisation measurements, *the analysing power* is maximum at $\theta = 90^o$. In Fig. 7 the region of $\pm 10^o$ around this optimal θ value is magnified. For $\theta = 90^o$ one has for any E_B the following Møller scattering relevant quantities:
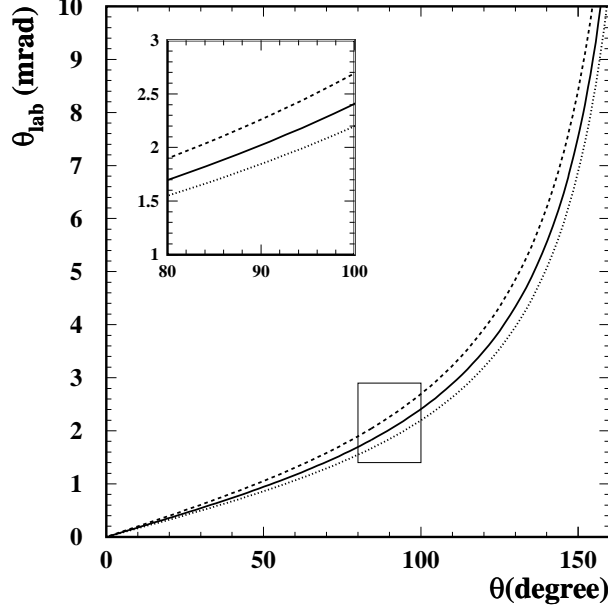
Figure 7: The Møller scattering angle in the laboratory system, θ_{lab}, as a function of θ, the CM angle. The target electron is at rest. The solid line is drawn for $E_B = 250$ GeV , the dashed one corresponds to $E_B = 200$ GeV and the dotted line is for $E_B = 300$ GeV . The insert magnifies the region where the scattering asymmetry is at or near its maximum.

$$A_L = \tfrac{7}{9}; \qquad A_t = \tfrac{1}{9} \quad \text{and} \quad A_R = -P_L^B P_L^T \times \tfrac{7}{9},$$

so that for $E_B = 250$ GeV one has:

$$d\sigma/d\cos\theta|_{\cos\theta=0} = 4.55(1 - 7/9 \times P_L^B P_L^T) \ \mu\text{barn} \quad , \qquad p_{lab} = 125 \text{ GeV} \quad \text{and}$$
$\theta_{lab} = 2$ mrad.

These variables are listed in Table 1 for several beam-target polarisation configurations.

3.2 Target electrons with non-zero momentum

In this subsection we evaluate the effects of the non-zero momenta of the target electrons on the quantities relevant to the Møller polarimetry. The target electrons are in fact not free particles at rest but are bound to atomic shells which

in the case of Fe atoms, move with a momentum in the range of $0 < p_T < 200$ keV [5]. The kinematic effects of these non-zero momentum target electrons are similar to those produced by the initial state radiation, namely the $e^- e^-$ CM energy is modified.

The detailed kinematics of the scattering of an energetic electron from a bound state electron moving with momentum p_T is discussed in [14]. To leading order, the CM energy is given by :

$$s = s_0 \left(1 - \frac{\vec{p}_T \cdot \vec{n}}{m_e} \right) \ , \tag{16}$$

where $\vec{p}_T$ is the momentum of the target particle and $\vec{n} = \vec{p}_B / p_B$ is the unitary vector pointing in the direction of the beam particle momentum. The presence of non-zero momentum target electron does not modify Eq. 13 but Eq. 15 is changed producing the Levchuk effect namely, the line image in $\theta_{lab} - 1/p_{lab}$ space is broader.

Taking into account the corrected CM energy given by Eq. 16, one has to modify Eq. 15 to read:

$$\theta_{lab}^2 = 2m_e \left(\frac{1}{p_{lab}} - \frac{1}{p_B} \right) \left(1 \pm \frac{p_T}{m_e} \right) \ . \tag{17}$$

The laboratory scattering angle is smeared by the square root of the target momentum dependent factor $1 \pm p_T / m_e$, the same factor which modifies the CM energy.

In the experiments which operated during the last decade the targets used for the Møller polarimeters have been Fe alloy or pure Fe foils [5, 7, 8]. In these kind of materials the K- and L-shell electrons are unpolarised (with mean momentum of 90 keV and 30 keV) and the polarised ones reside in the M- and N-shells (with 10 keV and 2 keV average momenta). Only two electrons from the M-shell carry the Fe magnetization, out of a total of 26, yielding a maximum target polarisation of 8%.

For the polarised target electrons the smearing factor is small but for unpolarised electrons it can achieve values around 20%. In Fig. 8 we show the dependence of the scattering angle, θ_{lab}, on the CM angle θ for the case of target electrons at
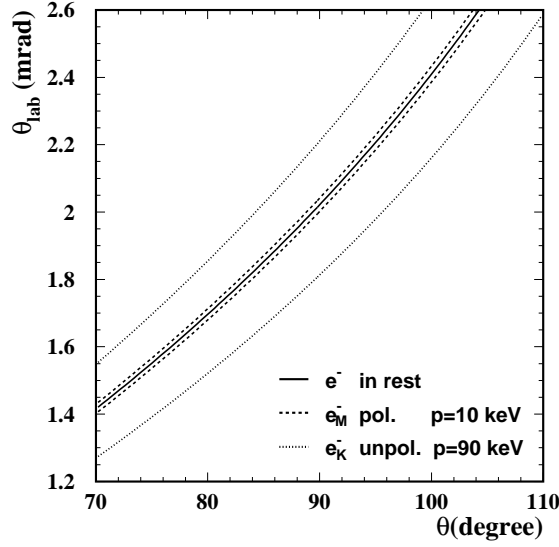
13

Figure 8: The Møller scattering angle, θ_{lab}, in the laboratory system as a function of θ, the centre of mass angle, for $E_B = 250$ GeV. The solid line is for the target electrons at rest and other two lines are for electrons from M and K atomic shells having a momentum of 10 and 90 keV.

rest (solid line) and for moving target electrons from the M and K shells (dashed and dotted lines).

In Fig. 9 we plot the momentum of elastic scattered Møller electrons as a function of θ, the centre of mass angle, for $E_B = 250$ GeV. As mentioned earlier, the momentum does not depend on s, the total CM energy squared (see Eq. 13) , therefore it is not modified even when the Fermi motion of the target electrons are accounted for. This means that the lines shown in Fig. 9 are not affected by the Fermi motion of the electrons and have not to be split for M and K atomic shells as is the case in Fig. 8.

In the case where the electron has a non-zero momentum, the CM energy squared s is given by Eq. 5 using the appropriate β_T value. (Note that for target electron at rest $\beta_T = 0$ and one obtains the CM energy squared s_0). In order to evaluate the effect of the non-zero momentum target electrons we list in Table 2 the values for $E_T^{Kinetic}$, E_T^{Total} and β_T for several value of P_T and in Fig. 10 we plot $1/s = 1/[2E_B E_T(1 - \beta_B \beta_T \cos\theta_{1,2})]$ as a function of E_B for various p_T values
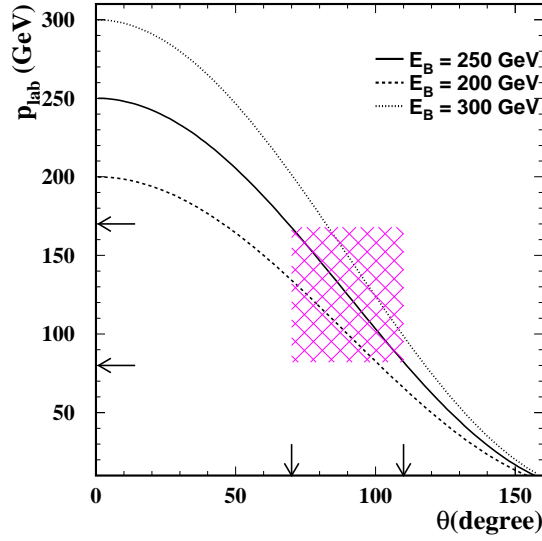
14

Figure 9: The Møller scattered electron momentum p$_{lab}$ in the laboratory system as a function of θ, the centre of mass angle, for various beam energy values. The optimal working region is shown by the hatched area.

setting $\beta_B = 1$ and $\cos\theta_{1,2} = -1$. From Fig. 10 follows that for $E_B = 250$ GeV the factor $1/s$, which enters in Eq. 1, changes by about 28% when the target electron momentum increases from 0 to 150 keV.

The effect on the asymmetry however is smaller, namely $10 - 15\%$ and can be estimated by using a proper simulation of the elastic Møller signal (see e.g. reference [5]). Finally the measured polarisation value is shifted by about 10% pending on the material of the target, the resolution and acceptance of the polarimeter and the analysis procedure.

The correction needed to account for this shift depends on the details of polarimeter construction, the beam parameters and analysis technique as is pointed out in [5]. At SLC the effect was found to be large due to the low emittance of the beam and the fine resolution of the detector. The solution to this problem, already adopted by E143 at SLC and JLAB [6,7] experiments, is given by adopting the coincidence measurement method using a double-arm polarimeter. These polarimeters have larger acceptance and poorer resolution so that the Levchuk effect was shown to be very small.

15

A recent study [15] on the performance of the double-arm polarimeter, has discovered a new effect arising from the Fermi motion of the atomic electrons in the target. Namely, that there exists a dependence of the measured Møller asymmetry on the relative position of the detectors in the double-arm operation mode. Here one should point out that the final decision and the technical design for a Møller polarimeter and the corresponding simulation of the apparatus and its performance have to be postponed until a final design of the collider will be available.
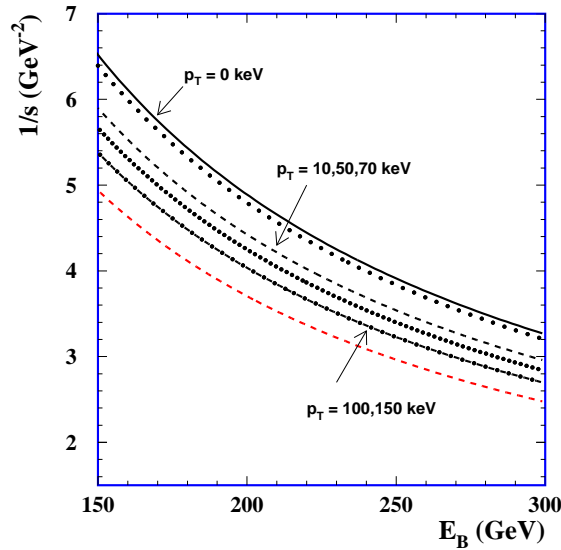
Figure 10: The variation of $1/s$ with beam energy for several values of the target electron momentum p_T.

4   Beam - Target related features

A technical drawing of the TESLA beam line section near the interaction point (IP), where a Møller polarimeter could in principle be placed, can be seen for example in Fig. 3.7.2 of Ref. [1], page 474. The final design and exact position of the Møller polarimeter however does depend on the choice taken between a single or a double arm device and on the detailed knowledge on the beam transport and background conditions. In these two possibilities the common elements of a

Møller polarimeter are:

- A magnetized target made usually of a Fe or Fe-alloy foil or if technological possible a new type of target (see e.g. Ref. [22]);
- A set of magnets to steer the scattered electrons;
- A collimator to define the accepted scattering range in the azimuthal angle ϕ and the ($\theta_{lab}^{min} - \theta_{lab}^{max}$) polar angle interval, for the elastic scattered electrons. This is followed by a dipole magnet that selects electron momenta in the desired range of acceptance;
- Finally the scattered electrons are detected and registered by an electromagnetic detector. To this end one can envisage for example a microstrip Silicon detector coupled to a electromagnetic calorimeter. This will enable to measure simultaneously the position and energy of the scattered electrons.

4.1 Expected luminosity

The current design of the TESLA beam consists of the set of parameters given in Ref. [1] and listed here in Table 3. This information is used here to evaluate *the effective luminosity*[5], the expected rate of Møller scattering events and its heating effect on the target due to the energy deposited by the electron beam. To this end we consider here the following target and electron beam features.

- For the target we take pure iron foil. The electron density ρ_e^{target} in such a pure iron target is:

$$\rho_e^{target} = N_A \cdot \rho \cdot \frac{\bar{Z}}{\bar{A}} \tag{18}$$

where N_A is the Avogadro number, ρ is the density of the material and $\bar{Z}, \bar{A}$ are the mean atomic number and atomic mass of the iron foil. Taking the density of this material to be $\rho = 7.87$ g/cm^3 and $\bar{Z}/\bar{A} = 466$ kg^{-1}, one obtains:

$$\rho_e^{target} = 2.21 \cdot 10^{24} \text{electrons/cm}^3. \tag{19}$$

- For the planned beam current of $I_{beam} = 45.2$ μA, the number of electrons which hit the target in a time interval of one second is:

---

[5]In the present context of fixed target scattering *the effective luminosity* is defined as the luminosity of the TESLA beam on the target electrons (see Eq. 21).

$$N_e^{beam} = \frac{I_{beam}}{q_e} = 2.82 \cdot 10^{14} \ \text{electrons/sec.} \tag{20}$$

4.2 Expected counting rates

The counting rate, defined as the number of Møller scattering events/sec, is given by:

$$\text{Rate} = d \times \rho_e^{target} \times N_e^{beam} \times \sigma_{mol} = \mathcal{L}_M \times \sigma_{mol} \tag{21}$$

where $\mathcal{L}_M$ is the so called effective luminosity. The Møller scattering cross section, σ_{mol}, is the result of the integration of Eq. 1 over the whole azimuthal angle range and over the CM polar angle θ domain $|\cos\theta| < 0.34$, chosen for our study, that is:

$$\sigma_{mol} = \int_0^{2\pi} d\phi \int_{-0.34}^{0.34} \frac{d\sigma}{d\cos\theta}(1 - P_L^B P_L^T A_L(\theta)) \ d\cos\theta \ , \tag{22}$$

where

$$\frac{d\sigma}{d\cos\theta} = \frac{\alpha^2}{s} \frac{(3 + \cos^2\theta)^2}{\sin^4\theta} \ .$$

Using the relevant values obtained in subsection 4.1, we evaluate for a high beam polarisation of 80% and a Fe target polarisation of 8%, namely $P_L^B P_L^T = 0.8 \times 0.08$, the cross section and effective luminosity to be:

$$\sigma_{mol} = 3.3 \cdot 10^{-30} \ \text{cm}^2 \quad \text{and} \quad \mathcal{L}_M = 6.2 \cdot 10^{35} \ \text{cm}^{-2}\text{sec}^{-1}.$$

From Eq. 21 the expected rate of Møller events is then:

$$\text{Rate} = 20.6 \cdot 10^5 \ \text{events/sec} \ .$$

One should point out that the numbers given here are summed over the whole ϕ angle range from 0 to 2π. In practice, the polarimeter acceptance covers only a small part of this range, denoted here by $\Delta\phi$. Therefore the last quoted rate has to be scaled down by the factor $\Delta\phi/2\pi$. For a polarimeter acceptance of $\Delta\phi = 2\pi/9$ rad and $\Delta\theta = 40^o$ the expected rate is

$$\text{Rate} = 2.28 \cdot 10^5 \ \text{events/sec} = 228 \ \text{kHz} \ ,$$

which is well within the range of the current capabilities of the data acquisition systems used for Møller polarimeters.

4.3 Target for precise Møller polarimetry

The target frequently used in Møller polarimeters consisted of thin foils of ferromagnetic alloy with the composition 49% Fe(Z=26, A=57.9), 49% Co(Z=27, A=58.9) and 2% Vanadium(Z=23, A=50.9) known under the name of Vanadium-Permendur alloy. It is magnetised *in-plane* using a pair of Helmholtz coils producing a small magnetic field of 0.01 Tesla. The foils are usually mounted under an angle of $\sim 20^o$ with respect to the beam. The disadvantages of a target with *in-plane* magnetisation [6] are: a poor knowledge of the target polarisation i.e. having an uncertainty of $\sim 1.5\% - 3.0\%$ as reported in Refs. [5, 6, 8, 9]; the demagnetisation due to the target heating is undetected and the target polarisation forms a non-zero angle (typically 20°) with the beam direction.

In order to achieve a precision measurements of the beam polarisation of 1% these limitations have to be overcome given their massive contributions to the systematic error of such method. A novel approach has been recently developed and put to use [7, 17]. This new target is made out of a thin *pure iron* foils polarised *out-of-plane* in saturation with a 4 Tesla magnetic field parallel to the electron beam. The online measurement of the relative foil polarisation during the polarimeter operation is carried out with a laser beam making use of the polar Kerr effect [17].

This new target design allows to reach an accuracy of 0.5% on the target polarisation and thus meets the precision beam polarisation measurements requested by TESLA. This precision, in fact, was obtained in the experiment which operated with an electron beam of few μA having the energies of 1-6 GeV at JLAB (see Ref. [7]).

4.4 The effect of target temperature rising

In this subsection we address the question of the target heating due to the energy deposited by the impinging beam and its possible effect on the polarimeter performance. To this end we consider a pure Fe foil target with a thickness of $d = 10\ \mu$m and an area of about 30 cm^2 so that the target material seen by the beam is $\widetilde{\rho} = d \times \rho = 7.87 \cdot 10^{-3}$ g/cm^2. The target, which is cooled down to

---

[6]In the theory of magnetism the 'magnetisation density' is used, which is related linearly with the electron polarisation of the ferro-magnetic material.

about 110 K, is polarised in saturation *out of plane*, so that when it is placed perpendicular to the beam direction the projected longitudinal polarisation of the target electrons is at its maximum[7].

4.4.1 Local heating per bunch

The TESLA beam design envisages a pulse cycle of 5 Hz. The duration of each pulse is ~ 1 msec followed by a pause of ~ 199 msec. Each pulse contains 2820 bunches of 1 psec length which succeeded every 337 nsec.

The ionisation energy loss in the target of one beam electron with an energy of 250 GeV, is $dE_{ion}/dx = 2.5 \cdot 10^6$ eV/g/cm^2 (see e.g. Ref [16]). The energy, E, deposited in the target by one bunch is:

$$E = \widetilde{\rho} \ \times \ dE_{ion}/dx \ \times \ N_e^{bunch} \ , \tag{23}$$

where N_e^{bunch} is the number of beam electrons in one bunch namely, $2 \cdot 10^{10}$. From Eq. 23 follows that the quantity of energy deposited in the target is $4 \cdot 10^{14}$ eV/bunch corresponding to $6.4 \cdot 10^{-5}$ J/bunch. The local temperature rise induced by this energy depends on the beam spot size at the position of the polarimeter. In the present design of the Beam Delivery System of TESLA a possible position for the Compton and Møller polarimeters is the straight section of the e$^-$ linac, some few hundred meters before the IP just outside the quads [18]. Within this straight section it is advantageous to place the Møller polarimeter in the region where the beam profile is the largest having the dimensions of about: $\sigma_x = 75\mu m$ and $\sigma_y = 7.5 \ \mu m$. For the heating calculations we then take the beam spot to be $\Delta x = 4 \times \sigma_x$ and $\Delta y = 4 \times \sigma_y$. The instantaneous temperature rise ΔT, of the target area hit by one beam bunch over that of the liquid nitrogen, is shown in Table 4. The ΔT values given in this Table are calculated for a pure iron target of 10 μm thickness taking the beam spot area to be $\Delta x \times \Delta y$ for several beam profile values.
In particular for the case $\sigma_x = 75 \ \mu m$ and $\sigma_y = 7.5 \ \mu m$, ΔT $= 200$ K.
From the values given in Table 4 it is obvious that the local temperature will be above the melting point[8] if all the bunches within one pulse will hit the same

---

[7]If the target is polarised *in plane* it has to be oriented at an angle ψ relative to the beam with the result that the longitudinal polarisation of the target electrons is reduced to $P_L^T = P^T \cdot \cos \psi$ and its effective thickness is increased to $d_{eff} = d/\sin \psi$.

[8]The Iron melting point is T $= 1808$ K.

small region of the target foil. To avoid this situation one needs to spread out over the target the individual hitting positions of the train of bunches. Such a solution is the subject of the next subsection.

4.4.2   The target cooling

In the present design of the next generation of Linear Colliders with large beam currents of 30 - 45 μA and high luminosity values the typical beam sizes are few tens of microns. Therefore when using for the beam polarisation measurements a Møller polarimeter, the local target heating requires a special care.

A possible solution to this local heating problem can be the implementation of a rotating disk target cooled down, all around its circumference, to about 110 K by liquid nitrogen. We note in passing that such a solution for the heating problem has been applied to a Møller polarimeter [19] which operated in an electron beam of 0.8 to 5.0 GeV with a current of 0.5 to 5.0 μA where the needed polarisation measurement time was about 20 min.

The envisaged target is placed in such a way that its rotation axis is parallel displaced to the beam direction so that successive bunches hit different regions of the target and in fact they will be distributed over a circle. Here we note that a rotating target has already been applied in the experiment described in Ref. [19]. If the disk rotates with a frequency of about 1000 Hz, around an axis displaced by 2.7 cm from the beam direction, all the impact points of the 2820 bunches of a single pulse, will be spaced by about 60 μm over an annular zone having a width of 300 μm.

Inasmuch that one can neglect the interference effects of one heated point by the others we evaluate, using the well known heat conduction formulae [20], that each heated spot will be cooled down within about 2 msec to 0.1 K above the liquid nitrogen temperature. This short time is mainly determined by the shortest distance to the cooled edge of the target. The residual heating of about 0.5 K/sec results in a final temperature rise of 50 K at the end of a 80 sec operation time needed for a polarisation measurement with a precision of about 1 % . Finally the fact that the pause between pulses is even 199 msec one has a sufficient safety margin to cover possible additional minor factors which may affect the cooling

time calculations.

The local rise in temperature of about 200 K, causes a relatively negligible target depolarisation since the working point at $\sim$ 110 K lies in the plateau region of the magnetisation curve shown in Fig. 11.
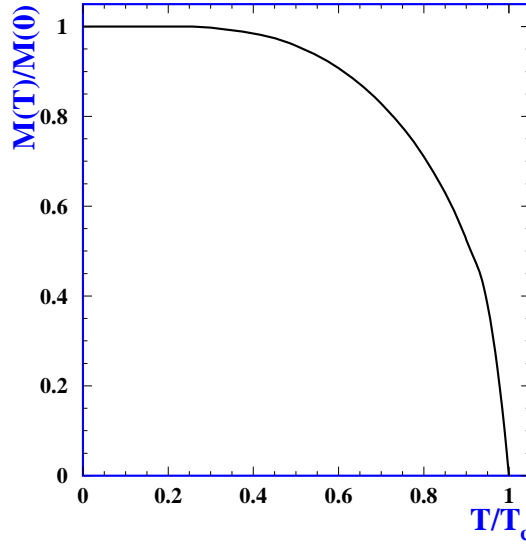

Figure 11: Saturation magnetisation of Fe as a function of the temperature scaled by the Curie temperature $T_c = 1043$ K.

This curve is derived from equation

$$M(T) \;=\; M(0)\tanh\left(\frac{M(T)}{M(0)} \times \frac{T_c}{T}\right) \tag{24}$$

which describes the magnetisation M of the material as a function of T/T_c where T_c is the Curie temperature, e.g. 1043 K for Fe (see e.g. [21]). For temperatures above T_c the spontaneous magnetisation vanishes. As seen from Fig. 11 at room temperature ($\simeq 300$ K) or less, the magnetisation depends weakly on T. Assuming the cooling temperature of the target to be 110 K, the increase ΔT of the local temperature given in Table 4 corresponds to a change in the magnetisation of ΔM = 0.3 % for a beam profile of $\sigma_x\sigma_y = 75 \times 7.5$ μm^2. Thus the heating of the target does not damage its magnetisation and the corresponding polarisation characteristics.

5 Measurement of the beam polarisation

The level of the electron beam longitudinal polarisation P_L^B is extracted from the measured A_R asymmetry defined in Eq. 3, which is calculated from the results of the two measured rates obtained from the Møller scattering with two different relative orientations of the beam polarisation vector with respect to that of the target. To this end we consider two possible variations for the polarisation evaluation:

- **Integrated polarisation measurement**

  In this method the number of Møller scattering events is summed over the whole polarimeter acceptance region. If we denote by N_+ and N_- the recorded scattered events in the relative parallel and anti-parallel beam and target polarisation vectors, properly normalised and corrected for efficiency, then the measured A_R asymmetry is given by $(N_+ - N_-)/(N_+ + N_-)$. The final beam polarisation is then derived from this measured asymmetry and the known target polarisation.

- **Differential polarisation measurement**

  If the polarimeter is equipped with a detector which measures also the momentum of the Møller scattered electrons one is able not only to measure the total rate of the scattering events but also their momentum distribution. This allows a more precise measurement of P_L^B and facilitates a better control of possible systematic effects. Moreover it allows to optimise the the polarisation measurement even in those cases where the beam is tuned to an energy somewhat different from its nominal designed value, e.g. 250 GeV in TESLA. In the differential polarisation measurement one considers the momentum distribution of the scattered electrons. For a given set N_p of p_{lab} momentum bins the numbers n_+^i and n_-^i of the Møller electrons are counted. The asymmetry is calculated for each x_i bin and the beam polarisation $P_L^{B,i}$ is at first determined bin by bin. The weighted mean of these values provides the final value of the beam polarisation.

5.1 Integrated polarisation measurement

The numbers of elastic Møller scattering events are counted for two different relative beam-target polarisation vectors, namely $(\vec{P}^B, \vec{P}^T)$ and $(-\vec{P}^B, \vec{P}^T)$. The number of Møller events integrated over the range x_{min} to x_{max} where x is defined as:

$$x = 2p_{lab}/E_B$$

and summed over the measurement time T_+ and T_- are given by:

$$N_+ \; = \; \mathcal{L}_+ T_+ \int_{x_{min}}^{x_{max}} \varepsilon_+(x) \frac{d\sigma}{dx}(1 - P_L^B P_L^T A_L(x))dx \,, \qquad (25)$$

$$N_- \; = \; \mathcal{L}_- T_- \int_{x_{min}}^{x_{max}} \varepsilon_-(x) \frac{d\sigma}{dx}(1 + P_L^B P_L^T A_L(x))dx \,, \qquad (26)$$

where $\varepsilon_+(x)$ and $\varepsilon_-(x)$ describe the efficiencies of the polarimeter as a function of x and $\mathcal{L}_+$ and $\mathcal{L}_-$ are the luminosity values for the parallel and anti-parallel beam-target spin states. The functions $d\sigma/dx$ and $A_L(x)$ are the unpolarised Møller cross section and the asymmetry. These are given by the expressions:

$$\frac{d\sigma}{dx} \; = \; \frac{2\pi\alpha^2}{s} \frac{[3 + (x-1)^2]^2}{[1 - (x-1)^2]^2} \; ; \qquad (27)$$

$$A_L(x) \; = \; \frac{[7 + (x-1)^2][1 - (x-1)^2]}{[3 + (x-1)^2]^2} \; . \qquad (28)$$

Eqs. 27 and 28 are derived from Eqs. 1, 2 and the relation 13 after integration over the whole azimuthal angle range.

To evaluate the polarimeter performance we choose our optimal measurement domain the one shown by the stripped area in Fig. 9, which confines the x range to the limits $x_{min} = 0.66$ and $x_{max} = 1.34$. For simplicity we consider the case where the integrated luminosities and efficiencies for the parallel and anti-parallel polarisations of the beam and target electrons are the same i.e., $\mathcal{L}_+ T_+ = \mathcal{L}_- T_-$ and $\varepsilon_+(x) = \varepsilon_-(x) = \varepsilon(x)$. The experimental measured asymmetry A_{exp} is written as:

$$A_{exp} = \frac{N_+ - N_-}{N_+ + N_-} = P_L^B P_L^T < A_L > \,, \qquad (29)$$

where the mean value $< A_L >$ is given by:

$$< A_L >= \frac{\int \varepsilon(x) \frac{d\sigma}{dx} A_L(x)dx}{\int \varepsilon(x) \frac{d\sigma}{dx}dx} \; . \qquad (30)$$

Thus the beam polarisation,

$$P_L^B = \frac{A_{exp}}{P_L^T < A_L >} , \qquad (31)$$

is proportional to the inverse of the mean longitudinal asymmetry. The relative error of the measured beam polarisation P_L^B is evaluated from Eq. 31 to be:

$$\left(\frac{\Delta P_L^B}{P_L^B}\right)^2 = \left(\frac{\Delta A_{exp}}{A_{exp}}\right)^2 + \left(\frac{\Delta P_L^T}{P_L^T}\right)^2 , \qquad (32)$$

where the error on the measured asymmetry is :

$$\Delta A_{exp}^2 = 4\frac{N_+ N_-}{N^3} = \frac{1 - A_{exp}^2}{N} = \frac{1}{\mathcal{L}T\sigma_t}\left(1 - (P_L^B P_L^T < A_L >)^2\right) . \qquad (33)$$

Here N is the total scattering events number recorded within the domain $x_{min} - x_{max}$ i.e.,

$$N = N_+ + N_- = \mathcal{L} \cdot T \cdot \sigma_t ,$$

with

$$\sigma_t = \int_{x_{min}}^{x_{max}} \varepsilon(x)\frac{d\sigma}{dx}dx \cdot$$

By using Eqs. 33 and 31 we can rewrite Eq. 32 as follows:

$$\left(\frac{\Delta P_L^B}{P_L^B}\right)^2 = \frac{1}{\mathcal{L}T\sigma_t}\frac{1 - (P_L^B P_L^T < A_L >)^2}{(P_L^B P_L^T < A_L >)^2} + \left(\frac{\Delta P_L^T}{P_L^T}\right)^2 . \qquad (34)$$

Since the term $(P_L^B P_L^T < A_L >)^2$ is $\leq 2.4 \cdot 10^{-3}$ (see Table 4), it is negligible in comparison to 1, so that one can simplify Eq. 34 to:

$$\left(\frac{\Delta P_L^B}{P_L^B}\right)^2 \simeq \frac{1}{\mathcal{L}T\sigma_t}\frac{1}{(P_L^B P_L^T < A_L >)^2} + \left(\frac{\Delta P_L^T}{P_L^T}\right)^2 . \qquad (35)$$

Thus the time t_{Int} needed to reach a desired relative polarisation precision $\Delta P_L^B/P_L^B$ is given by:

$$\frac{1}{t_{Int}} \simeq \mathcal{L}\left[\left(\frac{\Delta P_L^B}{P_L^B}\right)^2 - \left(\frac{\Delta P_L^T}{P_L^T}\right)^2\right]\left(P_L^B P_L^T\right)^2 \sigma_t < A_L >^2, \qquad (36)$$

which corresponds to the number of scattering events

$$N_{Int} = \mathcal{L} \times t_{Int} \times \sigma_t \qquad (37)$$

25

needed to perform the polarisation measurement. In Table 5 we present the characteristic unpolarised cross section and the averaged asymmetry values for several $x_{min} - x_{max}$ regions around $\theta = 90^o$ which may be of interest in a Møller polarimeter design. In Table 6 we list some of the values concerning the characteristics and performance of a TESLA Møller polarimeter. Using Eqs. 29 and 33 and the values listed in columns 1 to 3 of the Table 6, we calculated the number of events needed to obtain a relative statistical error of 0.5% for the measured asymmetry A_{exp}. From this we obtain the needed number of events and the corresponding run duration for a beam polarisation measurement with a relative error of about 1% which includes an assumed over-all 0.85 % systematic which includes also the uncertainty in the target polarisation level. These values are shown in the last two columns of Table 6. The precision expected from the TESLA polarimeter in a measurement duration of 80 sec is compared in Table 7 with three existing Møller polarimeters attached to high energy electron accelerators.

5.2 Differential polarisation measurement

The distribution of the measured momentum of the Møller scattered electrons is grouped in several x_i regions. In each region the recorded Møller scattering events with parallel and anti-parallel spin configurations are given by:

$$n_+^i = \mathcal{L}_+ T_+ \int_{x_i}^{x_{i+1}} \varepsilon_+(x) \frac{d\sigma}{dx} (1 - P_L^B P_L^T A_L(x)) dx \tag{38}$$

$$n_-^i = \mathcal{L}_- T_- \int_{x_i}^{x_{i+1}} \varepsilon_-(x) \frac{d\sigma}{dx} (1 + P_L^B P_L^T A_L(x)) dx \tag{39}$$

where $d\sigma/dx$ and A_L are the unpolarised Møller cross section and the asymmetry given in Eqs. 27 and 28.

The experimental asymmetry, in a given x_i bin, is expressed in terms of the beam and target polarisations as:

$$A_{exp}^i = \frac{n_+^i - n_-^i}{n_+^i + n_-^i} = P_L^{B,i} P_L^T < A_L >^i \tag{40}$$

As previously this formula is for the case where the integrated luminosities and efficiencies for the parallel and the anti-parallel electrons polarisation are identical. Specifically this means $\mathcal{L}_+ T_+ = \mathcal{L}_- T_-$ and $\varepsilon_+ = \varepsilon_-$.

26

For each bin one can then evaluate the beam polarisation as:

$$P_L^{B,i} = \frac{A_{exp}^i}{P_L^T < A_L >^i} \ .$$

(41)

The final beam polarisation is obtained as the weighted mean of the measured polarisations $P_L^{B,i}$, i.e.:

$$P_L^B = \sum_{i=1}^{N_p} \frac{P_L^{B,i}}{\Delta^2 P_L^{B,i}} \ / \ \sum_{i=1}^{N_p} \frac{1}{\Delta^2 P_L^{B,i}}.$$

(42)

The calculation of the relative error, $\Delta P_L^B / P_L^B$, follows very closely the one done before for the integrated polarisation measurement. Next we derived an expression for the needed time t_{Diff} to achieve a requested polarisation measurement accuracy of $\Delta P_L^B / P_L^B$, namely:

$$\frac{1}{t_{Diff}} \simeq \mathcal{L} \left[\left(\frac{\Delta P_L^B}{P_L^B} \right)^2 - \left(\frac{\Delta P_L^T}{P_L^T} \right)^2 \right] \left(P_L^B P_L^T \right)^2 \sigma_t < A_L^2 > \ .$$

(43)

which translates to the needed scattering events

$$N_{Diff} = \mathcal{L} \times t_{Diff} \times \sigma_t \ .$$

(44)

Here it should be noted that in the differential method a somewhat smaller number of events is needed to achieve the same precision for the relative P_L^B measurement. Another advantage of this method is the fact that it permits a better control on systematic errors and background contributions.

Above all the differential polarisation measurement allows to handle also cases where the linear collider runs at beam energies slightly away from the nominal designed beam energy, which in the TESLA case is 250 GeV. In fact one cannot exclude the necessity to operate the collider at beam energies away by several GeV from the nominal value due to technical problems or physics needs. If the beam energy changes the p_{lab} value corresponding to $\theta = 90^o$ is moving and therefore a momentum measurement of the Møller scattered electrons will still allow to utilise those scattered events which yield the maximum precision. This is best illustrated in Fig. 12 where in the plane of θ_{lab} versus p_{lab} the position of the 90° centre of mass scattering angle is shown for several beam energies around the nominal TESLA value of 250 GeV.
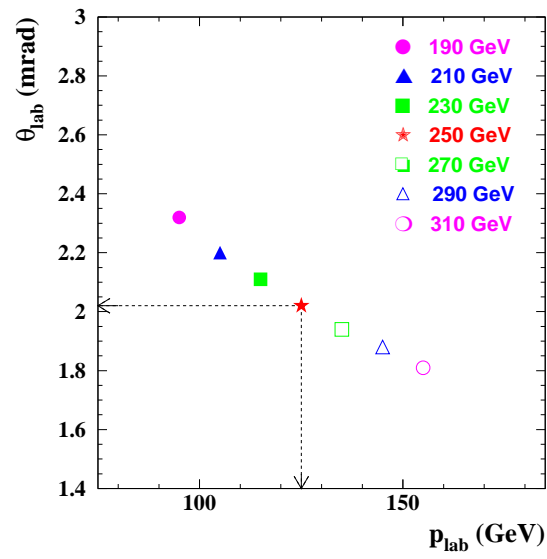
Figure 12: The values of θ_{lab} and p_{lab} in the laboratory system which correspond to the 90° centre of mass Møller scattering for several beam energies around the TESLA nominal value of 250 GeV.

Acknowledgments

References

[1] *Conceptual Design of a 500 GeV e^+e^- Linear Collider with Integrated X-ray Facility*, Eds. R. Brinkmann, G. Materlik, J. Rossbach and A. Wagner, Vol. I and II, DESY 1997-048 and ECFA 1997-182.

[2] see e.g. R. CasalBuoni et al., *Study of the anomalous couplings at NLC with polarized beams*, hep-ph/9912377;
A.A. Babich et al., *Contact interaction probes at the Linear Collider with polarized electron and positron beams*, Phys. Lett **B481** (2000) 263;
G.J. Gounaris, C.G. Papadopoulos, *Studying Trilinear Gauge Couplings at Linear Collider Energies*, Eur. Phys J. **C2** (1998) 365;
M. Woods, *Polarimetry at a future linear collider - how precise?*, SLAC-PUB-8397, hep-ex/0004004.

[3] H. Olsen, *Applications of Quantum Electrodynamics*, Springer Tracks in Modern Physics Vol. 44 (1968).

[4] M. Swartz, *Polarization at SLAC*, in "Polarization at LEP",
Eds. G. Alexander et al., CERN Yellow report 88-06, Vol. 2, p. 163.

[5] M. Swartz et al., *Observation of Target Electron Momentum Effects in Single-Arm Møller Polarimetry*, Nucl. Inst. and Meth. **A363** (1995) 526.

[6] P. Steiner, A. Feltham, I. Sick et al., *A high-rate coincidence Møller polarimeter*, Nucl. Inst. and Meth. **A419** (1998) 105.

[7] M. Hauger et al., *A high-precision polarimeter*, nucl-ex/9910013.

[8] J. Arrington et al., *A variable energy Møller polarimeter in the MIT-Bates Linear Accelerator Center*, Nucl. Inst. and Meth. **A311** (1992) 39.

[9] H.R. Band et al., *A Møller polarimeter for high energy electron beams (single-arm)*, Nucl. Inst. and Meth. **A400** (1997) 24.

[10] Spin Muon Collab., *Measurement of the SMC Muon Beam Polarisation using the asymmetry in the elastic scattering of polarised electrons*, CERN-EP-99-090, sub. to Nucl. Inst. and Meth.;
E. Burtin, *Mesure de la polarisation d'un faisceau de muons de 190 GeV par diffusion sur une cible d'electrons polarises*, Ph. D. Thesis, University Paris XI, Orsay, (1996).

[11] L.L. DeRaad Jr. and Y.J. Ng, *Electron-electron scattering. III. Helicity cross sections for electron-electron scattering*, Phys. Rev. **D11** (1975) 1586.

[12] N.M. Shumeiko and J.G. Suarez, *Radiative corrections to Møller Scattering of Polarized Particles*, hep-ph/9712407 and hep-ph/9912228.

[13] S. Jadach and B.F.L. Ward, *Multiple photon Monte Carlo simulation for polarized Møller scattering with Yennie-Fraustchi-Suura exponentiation at high energies*, Phys. Rev. **D54** (1996) 743.

[14] L.G. Levchuk, *The intra-atomic motion of bound electrons as a possible source of the systematic error in electron beam polarization measurements by means of a Møller polarimeter*, Nucl. Inst. and Meth. **A345** (1994) 496.

[15] A. Afanasev and A. Glamazdin, *Atomic electron motion for Møller polarimetry in a double-arm mode*, CEBAF-PR-96-003, hep-ex/9602002.

[16] Particle Data Group, *Review of Particle Physics*, Eur. Phys. J. **C15** (2000) 164.

[17] L.V. de Bever et al., *A target for precise Møller polarimetry*, Nucl. Inst. and Meth. **A400** (1997) 379.

[18] K.P. Schüler, *Polarimetry at TESLA* , Talk given at the 6th Linear Collider Workshop, May 2000, Padova, Italy.

[19] A.V. Glamazdin et al., *Electron beam Møller polarimeter at JLAB hall A*, hep-ex/9912063.

[20] See e.g., H. Stöcker, *Taschenbuch der Physik*, 3., Auflage, (Verlag Harri Deutsch), 1998, Section 22.10.
U. Grigull and H. Sandner, *Heat Conduction*, (International Series in Heat and Mass Transfer).

[21] C. Kittel, *Introduction to solid state physics*, 6th edition, (John Wiley & Sons Inc.) p. 426.

[22] *Polarised Protons at high Energies Accelerator Challenges and Physics Opportunities,* DESY-PROC-99-03.

$P_L^B \cdot P_L^T$	θ [degrees]	θ_{lab} [mrad]	$d\sigma/d\cos\theta$ [μbarn]	$\mathbf{A}_R$
$0.0 \cdot 0.0$	90°	2	4.6	0.0
$0.9 \cdot 0.9$	90°	2	1.7	0.63
$0.8 \cdot 0.08$	90°	2	4.4	0.05

Table 1: Some relevant parameters of a Møller polarimeter designed for a 250 GeV electron beam operated at centre of mass angle $\theta = 90^o$ i.e., at its maximum analysing power.

$E_T^{Kinetic}$ [keV]	E_T^{Total} [keV]	β_T	p_T [keV]
0.0	511.0	0.00	0.0
0.1	511.1	0.02	10.0
2.4	513.4	0.10	50.0
5.0	516.0	0.14	72.0
10.0	521.0	0.19	102.0
20.0	531.0	0.27	144.0

Table 2: The electron features of an iron target. The polarised electrons are in the M-shell having a momentum in the range $0 < p_T < 75$ keV with a maximum at 10 keV.

Beam Energy (E_B)	[GeV]	250.0
$\gamma = E_B/mc^2$ (for e)		4.89×10^5
Horizontal emittance	[m]	2.04×10^{-11}
Vertical emittance	[m]	6.13×10^{-14}
Horizontal normalized emittance	[μm]	10.0
Vertical normalized emittance	[μm]	0.03
Bunch length at IP	[mm]	0.3
Bunch population		2.0×10^{10}
Number of bunches		2820
Bunch separation	[ns]	337
Repetition Rate	[Hz]	5.0
Averaged current	[μA]	45.2

Table 3: TESLA beam characteristics.

$\Delta x \Delta y [\mu m^2]$	400×40	320×30	300×30	240×30
ΔT [^{o}C]	113	188	200	250

Table 4: The instantaneous local temperature rise ΔT [^{o}C], of the target within the beam spot $\Delta x \Delta y$ during one bunch of ~ 1 ps before the heat is spread over the target.

θ_{CM} [degree]	90 ± 10	$\mathbf{90 \pm 20}$	90 ± 30	90 ± 40	90 ± 50
θ_{lab} [mrad]	$1.70 - 2.41$	$\mathbf{1.42 - 2.89}$	$1.17 - 3.50$	$0.94 - 4.33$	$0.74 - 5.56$
$x_{max} - x_{min}$	$1.17 - 0.83$	$\mathbf{1.34 - 0.66}$	$1.5 - 0.5$	$1.64 - 0.36$	$1.76 - 0.26$
$\sigma_t[2\pi\alpha^2/s]$	3.336	**6.831**	11.667	18.624	32.404
$< A_L >$	0.765	**0.730**	0.668	0.583	0.459
$< A_L^2 >$	0.585	**0.534**	0.453	0.357	0.242
$\frac{<A_L^2>-<A_L>^2}{<A_L^2>}$	0.1%	**0.3%**	2%	5%	13%

Table 5: The characteristic unpolarised cross sections and average asymmetries for Møller scattering calculated for $E_B = 250$ GeV. The boldface values are for the optimal working range marked in Fig. 9.

$\mathbf{P_L^B \cdot P_L^T}$	σ [μbarn]	$< \mathbf{A_R} >$	$\mathbf{\Delta P_L^B/P_L^B}$	$\mathbf{t_{Int}}$ [sec]	$\mathbf{N_{events}}$
$0.8 \cdot 0.5$	0.274	0.292	1.0%	2	$4 \cdot 10^5$
$0.8 \cdot 0.2$	0.342	0.117	1.0%	12	$3 \cdot 10^6$
$0.8 \cdot 0.1$	0.364	0.058	1.0%	53	$12 \cdot 10^6$
$0.8 \cdot 0.08$	0.369	0.047	1.0%	79	$18 \cdot 10^6$

Table 6: The characteristics and performance of a Møller polarimeter operated in the integrated polarisation measurement mode calculated for $E_B = 250$ GeV , $\Delta P_L^T/P_L^T = 0.5\%$, an x acceptance in the region of $x_{min} - x_{max} = 0.66 - 1.34$ and $\Delta\phi = 40^o$. The values given are for 100% efficiency.

	JLAB [7]	E143 at SLC [6]	SLD at SLC [5]	TESLA
Target	Fe	Fe+Co Alloy	Fe+Co Alloy	Fe
E_B [GeV]	$1-6$	16 & 29	46.6	250
θ_{lab} [mrad]	$32-13$	8 & 6	4.5	2.0
p_{lab} [GeV]	$0.5-3$	8 & 14.5	23.3	125.0
$(\Delta P_e)_{syst}$	0.5 %	2.6 %	3.4 %	0.85 %$_{assumed}$
$\Delta P_e/P_e$	$\simeq 1.3$ %	$\simeq 3.7$ %	$\simeq 4.2$ %	1.0%

Table 7: A compilation of several relevant parameters of three existing Møller polarimeters, at high energy electron experiments, compared to a feasible polarimeter configuration for TESLA. The θ_{lab} and p_{lab} values are calculated for $\theta = 90^o$. The precision of the longitudinal beam polarisation measurements $\Delta P_e/P_e$ is also listed. The value of $\Delta P_e/P_e = 1.0$ % given to TESLA corresponds to a measurement duration of 80 sec (see Table 6) assuming a 0.85 % systematic error.